Available online at www.sciencedirect.com
SCIENCE DIRECT®
Tetrahedron: Asymmetry
Tetrahedron: *Asymmetry* 15 (2004) 3103–3109

Chiral matrix effect of optically active oxalate-based networks: controlled helical conformation of an organic chromophore

Michel Gruselle,[a,*] Bernard Malézieux,[a] Sophie Bénard,[c] Cyrille Train,[a] Carine Guyard-Duhayon,[a] Patrick Gredin,[b] Kaia Tonsuaadu[d] and René Clément[c]

[a]*Laboratoire de Chimie Inorganique et Matériaux Moléculaires, UMR 7071, Université Pierre et Marie Curie, 4 place Jussieu, case 42, F-75252 Paris Cedex 05, France*
[b]*Laboratoire de Cristallochimie du Solide, Université Pierre et Marie Curie, 4 place Jussieu, case courrier 176, F-75252 Paris Cedex 05, France*
[c]*Laboratoire de Chimie Inorganique, UMR 8613, Université Paris Sud, 91405 Orsay Cedex, France*
[d]*Institute of Chemical Engineering, Tallinn Technical University, Ehitajate tee 5, 19086 Tallinn, Estonia*

Received 24 June 2004; accepted 28 July 2004

Abstract—Optically active two-dimensional (2D) MIPS[$Mn^{II}M^{III}(C_2O_4)_3$] bimetallic networks with MIPS = 4-[4-methoxy-α-styryl]-*N*-isopentylpyridinium and M^{III} = Cr, Co were obtained using as chiral inducing reagents the resolved (Δ)- or (Λ)-$[M^{III}(C_2O_4)_3]^{3-}$ building blocks. The correlation of the natural circular dichroism (NCD) of these 2D networks with their UV–vis properties demonstrates that the $[Mn^{II}M^{III}(C_2O_4)_3]^-$ anionic network has a chiral matrix effect on the $MIPS^+$ cation: the choice of the configuration of the starting tris(oxalato)metallate(III) determines the helical conformation of the $MIPS^+$ cation. Such a conformation of the cation sharply contrasts with the perfectly planar geometry observed by X-ray diffraction in MIPSBr.

1. Introduction

Nonlinear optical (NLO) effects of organic chromophores have been widely studied in solution.[1] Few attempts have been made to obtain these effects in the solid state by inserting the chromophore in inorganic matrices.[2–6] Nevertheless a centrosymmetric arrangement of the NLO chromophores in the crystal often wrecks this approach because it leads to an exact cancellation of the NLO effects.

Two-dimensional (2D) bimetallic oxalate-based networks of general formula: $C[M_1^{II}M_2^{III}(ox)_3]$ ($ox = C_2O_4^{2-}$) noted $C[M_1^{II}–M_2^{III}]$ where C is a monocation and M_1, M_2 two transition metal ions appear as interesting candidates to pertain NLO effects in the solid state. The 2D $[M_1^{II}M_2^{III}(ox)_3]^-$ matrix exhibits a honeycomb structure. Within the network, the $M(ox)_3$ moiety presents a helical chirality. It can thus exists as (Δ) or (Λ) enantiomers. In a given $[M_1^{II}M_2^{III}(ox)_3]^-$ layer, the two metal ions are of opposite configuration. Nevertheless, because of different metal–ligand bond lengths for M_1 and M_2, each layer is chiral. Thus there can exist enantiospecific interactions between an anionic layer and the neighbouring cation. This has been recently exemplified for chiral ferrocenic ammonium inserted in such networks.[7] We aim to exploit such interactions to obtain non-centrosymmetric crystal structure and avoid a head-to-tail arrangement of the chromophore in the solid state in order to observe NLO effects. Moreover by a proper choice of the metal ions, we can obtain a material possessing NLO effects together with long range magnetic order at low temperature.[6]

Up to date, two centrosymmetric structures have been resolved for stilbazolium containing 2D oxalate-based ferromagnets starting from (*rac*)-$[Cr(ox)_3]^{3-}$.[4] In DAPS[Mn–Cr] (DAPS = 4-[4-(*N*,*N*-dimethylamino)-α-styryl]-*N*-isopropylpyridinium), the cations lie within the interlayer space. They are planar and adopt an edge-on arrangement. With the 4-[4-methoxy-α-styryl]-*N*-isopentylpyridinium (MIPS) cation, the situation is significantly different. One of the ethyl group of the

* Corresponding author. E-mail: gruselle@ccr.jussieu.fr

0957-4166/$ - see front matter © 2004 Elsevier Ltd. All rights reserved.
doi:10.1016/j.tetasy.2004.07.062

amino moiety enters one of the cell of the honeycomb of the anionic network and the cation is twisted around the C–C bonds connecting the two aromatic rings.[4]

For the well-studied TBA[Mn–M^{III}] (TBA = $N(^nC_4H_9)_4$, M = Cr, Co), when starting from (*rac*)-$[M^{III}(ox)_3]^{3-}$, the obtained material crystallises in the *R3c* space group. The alternation of the configuration of the $M(ox)_3$ moiety when going from one anionic plane to the other indeed leads to an achiral structure.[8] On the contrary, when starting from resolved (Δ)- or (Λ)-$[M^{III}(ox)_3]^{3-}$ (M = Cr, Co) anionic bricks, it is possible to obtain these networks in their optically active forms.[9,10] The material then crystallises in a non-centrosymmetric space group. The inversion centre is lost because all the anionic layers have the same configuration.

We present herein the enantioselective synthesis of MIPS[Mn–Cr], MIPS[Mn–Co] using resolved $[M^{III}(ox)_3]^{3-}$ (M = Cr, Co) as chiral inducing reagents. In such conditions, if the interaction between the cation and the anionic network is stereospecific, we expect that all the $MIPS^+$ cations adopt the same conformation. Natural circular dichroism (NCD) combined to UV–vis spectroscopy is used as the most direct probe of this phenomenon.

2. Results and discussion

2.1. Crystal structure of MIPSBr and comparison of the conformations of $MIPS^+$ in MIPSBr and MIPS[Mn–Cr]

Suitable crystals for X-ray diffraction of MIPSBr were obtained by slow evaporation of a water/ethanol solution. MIPSBr crystallises in the centrosymmetric *C2/c* space group. Crystallographic data are given in Table 1. The eight cations in the unit cell are paired in a head-to-tail manner with an intercationic distance of 3.4 Å suggesting strong π–π stacking interactions (Fig. 1). Such an arrangement prevents the appearance of any NLO in the solid state. The two aromatic rings are in the same plane allowing a good electronic delocalisation (Fig. 2a).

Table 1. Crystallographic data and diffraction parameters for MIPSBr

	MIPSBr
Formula	$(C_{19}H_{24}NO)\cdot(Br)\cdot(H_2O)_{1.5}$
M_r	389.33
Crystal size	$0.27 \times 0.35 \times 0.47$
Crystal system	Monoclinic
Space group	*C2/c*
a (Å)	19.033(5)
b (Å)	15.414(5)
c (Å)	13.831(5)
β (°)	102.77(2)
V (Å^3)	3957(2)
Z	8
ρ_{calcd} (g cm^{-3})	1.31
Temp (°C)	22
λ (Mo-K_α) (Å)	0.71069
μ (cm^{-1})	20.09
$R(F_o)$[a]	0.0521
$R_w(F_o)$[b]	0.0560

[a] $R = \sum(|F_o|-|F_c|)/\sum F_o$.
[b] $R_w = \left[\sum w(|F_o|-|F_c|)^2/\sum wF_o^2\right]^{1/2}$.

As shown by Bénard et al.[4], the situation is significantly different when the $MIPS^+$ cation is located in a layered $[MnCr(ox)_3]_n^{n-}$ matrix (Fig. 2b). In this case, it has a twisted conformation. The dihedral angle between the benzene and pyridinium rings being found as high as 30.8°.[4] From this twisting arises a helical chirality of the cation, which conformations can be labelled as (Δ) and (Λ). Moreover the $MIPS^+$ cation interacts with the $[Mn–Cr]^-$ anionic honeycomb layer through one of the ethyl chains of the *N*-isopentyl group (Fig. 3). These chains actually occupy two different positions. One is parallel to the anionic layers while the other penetrates one cell of the honeycomb layer. The Van der Waals interactions with the anionic layer are thus different for the two ethyl chains linked to the carbon atom bounded to the nitrogen atom. This prochiral carbon atom thus becomes stereogenic. A close look at the structure of the achiral MIPS[Mn–Cr] compound published by Bénard et al.[4] indicates that the MIPS cation interacting with a $[(\Lambda)\text{-Mn}-(\Delta)\text{-Cr}]^-$ anionic layer adopts the (*R*)-(Λ) configuration (Fig. 3) while (*S*)-(Δ)-MIPS is associated with $[(\Delta)\text{-Mn}-(\Lambda)\text{-Cr}]^-$ anionic layers.

In our opinion, in MIPS[Mn–Cr], the twisted conformation of the stilbazolium cation is the result of the specific interactions between the chiral anionic layer and the cation mediated by the prochiral carbon atom bound to the nitrogen atom of the MIPS cation.

Because the compound described by Bénard et al.[4] has been obtained starting from racemic tris(oxalato)chromate(III), both configuration of the metal ion are present in the compound as well as both enantiomers of the $MIPS^+$ cation and definitive conclusion cannot be drawn. To show the specificity of the interaction between the cation and the anionic network, we therefore decided to obtain MIPS[Mn–Cr] in its enantiomeric forms starting from resolved tris(oxalato)metallate(III).

2.2. Synthesis of optically active MIPS[Mn–Cr] and MIPS[Mn–Co] and TGA analysis

All the syntheses were performed using a mixture of water and methanol as solvent. Optically active 2D networks were obtained using optically active tris(oxalato)-chromate(III) or cobaltate(III). To avoid the racemisation of the anionic building, the syntheses were performed as rapidly as possible. Such an operating mode also prevents the formation of single crystals. TGA analysis showed no loss of solvent molecule. The studied compounds start to decompose above 225 °C, establishing the robustness of the oxalate-based architecture.

2.3. X-ray diffraction powder

The X-ray diffraction powder patterns were recorded for MIPS[Mn–Cr] and MIPS[Mn–Co] in their racemic and

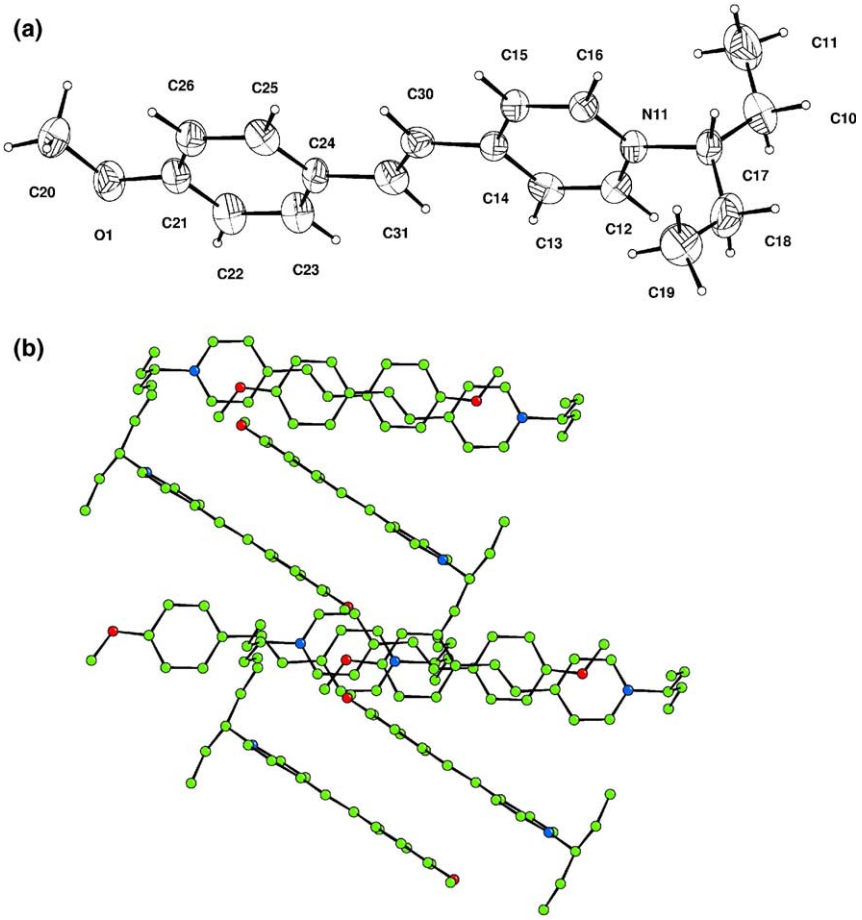

Figure 1. Molecular structure of MIPSBr with the atom numbering system (a), packing of MIPSBr in the crystal (b).

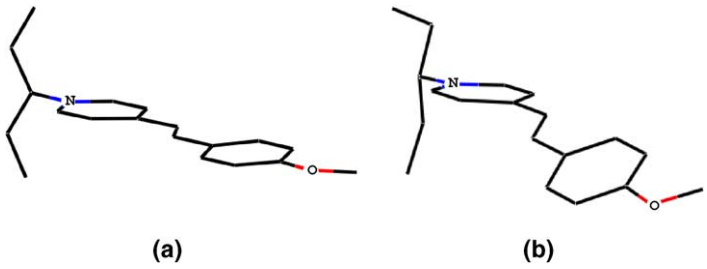

Figure 2. Comparison of the planar conformation of $MIPS^{+}$ in MIPSBr (current work) (a), helical conformation observed in (*rac*)-MIPS[Mn–Cr] (adapted from Ref. 4) (b).

optically active forms. Despite of a long counting time, the signal-to-noise ratio of the X-ray powder patterns remains low. This is due to a rather poor crystallinity correlated with the necessary fast rate of the reaction to avoid the racemisation of the starting building blocks. In such a situation, using Rietveld refinement to determine the position and the conformation of the MIPS cation with respect to the anionic layers would lead to unreliable conclusions. The exploitation of the X-ray powder diffraction patterns is thus limited to the determination of the cell parameters and the checking of the possible space groups. The X-ray powder diffraction patterns of the racemic compounds can be indexed in the monoclinic cell in the space group $P2_1/c$ according to the crystal structure of MIPS[$MnCr(ox)_3$] previously solved by Bénard et al.[4] The refined cell parameters are for MIPS[Mn–Cr]: $a = 9.524(2)$ Å, $b = 15.880(2)$ Å, $c = 18.228(4)$ Å, $\beta = 83.99(2)°$ and for MIPS[Mn–Co]: $a = 9.595(2)$ Å, $b = 15.973(3)$ Å, $c = 18.590(3)$ Å, $\beta = 82.69(2)°$. We obtain very comparable results for the optically active compounds. An important point is that the analysis of the diffraction pattern does not allow to distinguish between the centrosymmetric $P2_1/c$ and the chiral $P2_1$ space groups. Indeed, the use of one space group or the other in the calculation of the diffraction patterns does not lead to significant changes in the diffracted intensities that could be related to the observed X-ray patterns. Nevertheless the diffraction patterns establish the layered structure of both the racemic and optically active compounds.

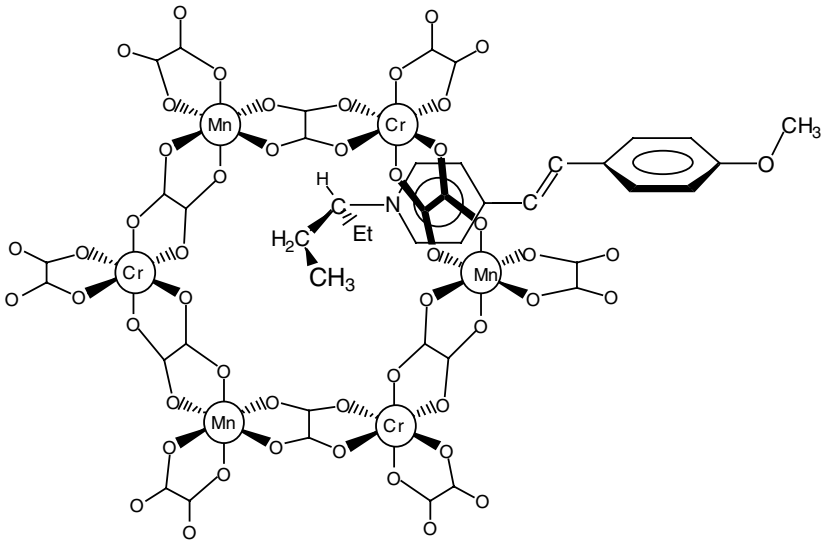

Figure 3. (*R*)-(Λ)-MIPS cation associated with a [(Λ)-Mn–(Δ)-Cr]$^-$ anionic layer.

2.4. UV–vis spectroscopy

Due to extremely low solubility of the compounds, solid state (KBr pellet) UV–vis spectroscopy was imposed. The spectra of MIPS[Mn–Cr] and MIPS[Mn–Co] are compared to those of MIPSBr and of the corresponding TBA[Mn–M] 2D network (Fig. 4). The spectrum of MIPSBr presents a broad absorption band whose maximum is located at 390 nm. When the stilbazolium cation is incorporated in an oxalate-based $[MnCr(ox)_3]^-$ network, the maximum is displaced from 390 to 410 nm and there appears a shoulder at 580/600 nm (Fig. 4a). When the stilbazolium cation is incorporated in a $[MnCo(ox)_3]^-$, no noticeable difference appears in the position of the maximum nor any deformation of the lineshape of the spectrum (Fig. 4b). Though solid state measurements introduce scattering effects that prevent a fully quantitative interpretation of the intensity of the band, the insertion of the stilbazolium cation in both oxalate-based network leads to a significant hyperchromic effect as compared to the corresponding bromide salt. According to Coradin et al. the shoulder observed for MIPS[Mn–Cr] (Fig. 4a) should be related to the formation of weak *J*-aggregates between inserted cationic species.[3]

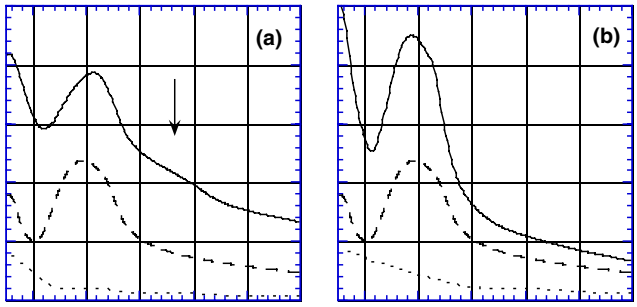

Figure 4. UV–vis spectra of MIPS[Mn-M] (—), MIPSBr (---) and TBA[MnM(ox)$_3$] (···) for M = Cr (a) and M = Co (b).

The UV–vis spectra of the stilbazolium derivative is dominated by intense charge-transfer bands with molar absorption coefficients ε in solution above $10^5\,L\,mol^{-1}\,cm^{-1}$. On the contrary, the UV–vis spectrum of tris(oxalato)chromate(III) containing solution is mainly associated to d–d transition of Cr(III) with molar absorption coefficient in water around $10^2\,L\,mol^{-1}\,cm^{-1}$.[11] As a consequence of the relative values of the molar absorption coefficients of the two chromophores, the evolution of the spectrum when going from stilbazolium halide to stilbazolium inserted in the oxalate-based network is not due to supplementary signals arising from the presence of the transition metal ions of the anionic network but to modifications of the absorption of the chromophore itself.

2.5. Natural circular dichroism

The natural circular dichroism (NCD) spectra measured on MIPS[Mn–Cr], MIPS[Mn–Co] obtained starting from either (Δ)- or (Λ)-$[M^{III}(ox)_3]^{3-}$ (M = Cr, Co) are shown in Figure 5. In both cases, the curves are of opposite signs, starting from the opposite configurations of the resolved tris(oxalato)metallate(III). For MIPS[Mn–Cr] and MIPS[Mn–Co], The NCD curves present three extrema at 334(+), 445(−), 572(+) nm starting from (Δ)-$[Cr(ox)_3]^{3-}$ (Fig. 5a) and at 342(+), 444(−), 640(−) nm starting from (Δ)-$[Co(ox)_3]^{3-}$ (Fig. 5b).

In order to assign different signals observed in the NCD spectra, the observed NCD transitions were correlated with those measured on the parent compounds TBA[Mn–Cr] and TBA[Mn–Co] and with the transitions observed in the UV–vis spectra (Fig. 4).

The NCD spectra of TBA[Mn–Cr] and TBA[Mn–Co] are dominated by a negative (respectively, positive) signal at 565 nm (respectively, 619 nm) when starting form (Δ)-$[Cr^{III}(ox)_3]^{3-}$ (respectively, (Λ)-$[Co^{III}(ox)_3]^{3-}$) (Fig. 5). These NCD signals are associated with d–d transi-

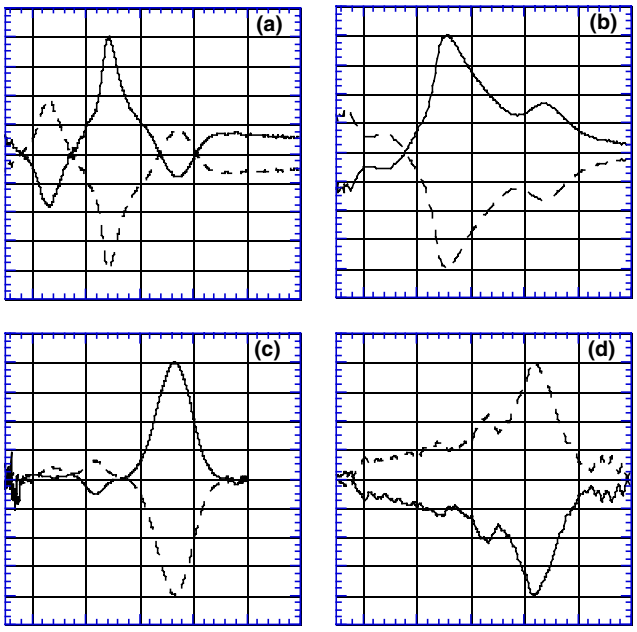

Figure 5. Natural circular dichroism for (a) MIPS[Mn–Cr]; (b) MIPS[Mn–Co]; (c) TBA[Mn–Cr]; (d) TBA[Mn–Co] obtained from (Λ)-$[M^{III}(ox)_3]^{3-}$ (—) or from (Δ)-$[M^{III}(ox)_3]^{3-}$ (---).

tions observed in the UV–vis spectra of these compounds at the same wavelengths.

For MIPS[Mn–(Δ)-Cr] and MIPS[Mn–(Δ)-Co], the most important feature of the NCD spectra appears at 445 and 458 nm, respectively. They do not correspond to any dichroism signal arising from the anionic network. According to the UV–vis spectra, they shall be associated with the charge-transfer transition in the MIPS cation. They are attributed to the twisting of the cation inserted in the material.

At first sight, the signals observed at 576 nm for MIPS[Mn–(Δ)-Cr] and 636 nm for MIPS[Mn–(Δ)-Co] could be associated to the d–d transition of the metal ion. Nevertheless, the maximum positions are slightly different and the signs are opposite to those observed in TBA[Mn–Cr] and TBA[Mn–Co]. Moreover they cannot be related to any particular feature of the UV–vis spectra (Fig. 4). Nevertheless, as exemplified in metal complexes, a broad band as the ones appearing in the UV–vis spectrum of MIPS[MnCr] and MIPS[MnCo] (Fig. 4) often leads to more detailed features in NCD.[12]

The fact that the NCD spectra are symmetric with respect to the *x*-axis when going from one enantiomer of the starting anionic building blocks to the other indicates that the configuration of the starting tris(oxalato)metallate(III) determines the twisted conformation of the MIPS cation inserted in the anionic network. The formation of 2D networks is thus enantioselective. Moreover since the signal around 450 nm has the same sign for the material obtained from $[(\Lambda)\text{-}Cr(ox)_3]^{3-}$ or from $[(\Lambda)\text{-}Co(ox)_3]^{3-}$ and that an opposite signal is observed starting from $[(\Delta)\text{-}Cr(ox)_3]^{3-}$ or from $[(\Delta)\text{-}Co(ox)_3]^{3-}$, we can conclude that the interaction between the cation and the anionic network is stereospecific. Taking into account the detailed analysis (Fig. 3) of the structure published by Bénard et al.[4] the positive signal observed around 450 nm for the material synthesised starting from $[(\Lambda)\text{-}Cr(ox)_3]^{3-}$ is attributed to (*S*)-(Δ)-MIPS while the negative signal is attributed to (*R*)-(Λ)-MIPS.

3. Concluding remarks

Along these lines, we have demonstrated the ability of 2D $[MnCr(C_2O_4)_3]^-$ anionic layers having a definite configuration to determine the absolute conformation of the MIPS cation inserted between the layers. This work thus highlights that the conformation of the stilbazolium cation is ruled by stereospecific interactions between one of the ethyl chain of the prochiral $-NC^*H(C_2H_5)_2$ carbon atom with the anionic network. This indicates that optically active oxalate-based network are promising matrices for observing NLO effects of incorporated hyperpolarisable stilbazolium in the solid state. Moreover, associating such NLO effects with the magnetic properties of the anionic networks will lead to fairly interesting multifunctional materials.

4. Experimental

The IR spectra were recorded on a Bio-Rad FTIR spectrometer as KBr pellets in the 250–4000 cm^{-1} region. Elemental analyses were completed at the SIARE-UPMC Paris. TGA experiments were performed with SETARAM TG/DTA LabSys 2000 equipment in an air flow 60 mL/min at heating rate 10 K/min in Pt crucible. The composition of the gases evolved was analysed simultaneously with FTIR gas analyser (Interspectrum). The gas cell with 8.8 m pathlength was maintained at 150 °C. Spectra were recorded in the 400–4000 cm^{-1} region.

UV–vis data were recorded between 250 and 800 nm on a UV-2101 PC Shimadzu spectrophotometer. The stilbazolium halide salts spectra in acetonitrile solution were measured using a 1 cm quartz cuvette. Solid state measurements were performed for stilbazolium bromide, its associated oxalate-based networks and for TBA[Mn-$M^{III}(ox)_3$] (M^{III} = Cr, Co; TBA = $N(^nC_4H_9)_4$) in KBr pellet using 0.2–2 mg of the desired compounds in 100 mg of KBr. All the solid state spectra were calibrated for a 10^{-4} mmol of chromophore (chromium(III), cobalt(III) or stilbazolium).

Specific rotations of the starting materials were measured at 20 °C in a 1 dm tube containing the aqueous solutions, using the sodium D line in a polarimeter Ameria AA5. The enantiomeric excesses were calculated by comparison to the maximum specific rotation found in the literature.[13,14] Natural circular dichroism (NCD) spectra were recorded with a Jasco model J-810 spectropolarimeter. Due to the extremely low solubility of the obtained polymers, NCD had to be measured using compounds in the solid state. Measurements were

performed on 13 mm standard diameter disks as dispersions of 0.1–1 mg of the resulting complexes in dried 100 mg KBr. The baseline correction was performed using the spectrum of pure KBr disk. Spectra were recorded over the wavelength range 250–800 nm. Because of scattering effects due to sample preparation and solid state measurement, this method is limited to qualitative comparison. The spectra have thus been normalised at the maximal signal observed in the studied spectral region.

4.1. Synthesis of starting materials

$K_3[Cr(ox)_3]\cdot 3H_2O$ and $K_3[Co(ox)_3]\cdot 3H_2O$ were prepared according to literature methods. Procedures of resolution already described have been followed to obtain Δ and Λ isomers of $[Cr(ox)_3]^{3-}$ and $[Co(ox)_3]^{3-}$.[13,14] (Δ)- or (Λ)-$K_3[Cr(ox)_3]\cdot 3H_2O$ $[\alpha]_D = -1780$ (*c* 0.040, H_2O) or $[\alpha]_D = +1558$ (*c* 0.040, H_2O), respectively. (Δ)- or (Λ)-$K_3[Co(ox)_3]\cdot 3H_2O$ $[\alpha]_D = +1575$ (*c* 0.025, H_2O) or $[\alpha]_D = -1472$ (*c* 0.025, H_2O), respectively. MIPSBr was obtained following previously reported methods.[4] The other reagents are commercially available and were used as purchased.

4.2. Synthesis of racemic MIPS[Mn–Cr] and MIPS[Mn–Co]

The same procedure, exemplified below for MIPS[Mn–Cr], has been followed to synthesise both compounds: A 0.25 mL water solution of $K_3[Cr(ox)_3]\cdot 3H_2O$ (34 mg, 0.072 mmol) and $MnCl_2\cdot 4H_2O$ (14 mg, 0.07 mmol) was poured into a methanolic solution of MIPSBr (26 mg, 0.072 mmol in 0.25 mL). After homogenisation, the mixture was rapidly filtered on a 0.4 μm polycarbonate membrane. Successive additions of methanol to the filtrate (3 × 2 mL) under rapid stirring led to the formation of a fine precipitate. The solid was filtered off using a 0.4 μm polycarbonate membrane, washed with pure methanol until the filtrate remains colourless and then dried after washing with 3 mL of diethyl ether. Thirty seven milligrams were recovered as a yellow-green microcrystalline powder (56% yield). IR (KBr pellet) 1631 cm^{-1}.

4.3. Synthesis of optically active MIPS[Mn–Cr] and MIPS[Mn–Co]

The procedure remains the same with the additional requirement that the configuration of the tris(oxalato)metallate has to be selected according to the target compounds.

IR: (KBr pellet) MIPS[Mn–Cr] 1631 cm^{-1}; MIPS[Mn–Co] 1626 cm^{-1}. The IR spectra are the same for the two enantiomers.

Analysis: MIPS[Mn–(Δ)-Cr], Calcd for $C_{25}H_{24}NO_{13}CrMn$: C 45.96, H 3.70, N 2.14. Found: C 42.82, H 3.38, N 1.48: MIPS[Mn–(Λ)-Cr]. Found: C 46.03, H 3.54, N 1.61. MIPS[Mn–(Δ)-Co], calcd for $C_{25}H_{24}NO_{13}CoMn$: C 45.47, H 3.66, N 2.12. Found: C 43.26, H 3.78, N 2.17.: MIPS[Mn–(Λ)-Co]. Found: C 46.10, H 3.54, N 2.15.

4.4. UV–vis spectra

Absorption maxima and molar absorption coefficient ε in acetonitrile of the stilbazolium bromide, MIPSBr: $\lambda_{max} = 383$ nm, 167,800 L mol^{-1} cm^{-1}. Absorption maxima in the solid state: MIPSBr: $\lambda_{max} = 390$ nm; MIPS[Mn–Cr]: $\lambda_{max} = 410$ nm; MIPS[Mn–Co]: $\lambda_{max} = 386$ nm.

4.5. Natural circular dichroism

MIPS[Mn–(Λ)-Cr]: 334(−), 445(+), 572(−); MIPS[Mn–(Λ)-Co]: 342(−), 444(+), 640(+).

4.6. X-ray diffraction

A yellow crystal of MIPSBr obtained by slow evaporation of a water/ethanol solution was mounted on a glass fibre. Measurements were performed on a Enraf–Nonius Cad-4 diffractometer, Mo-K_α radiation ($\lambda = 0.71069$ Å), collection range $2\theta = 2$–52°. Accurate cell dimensions and orientation matrix were obtained by least-squares refinement of 25 accurately centred reflections. The data were corrected for Lorentz and polarisation effects. Computations were performed by using Crystals 2000 version. Scattering factors and corrections for anomalous dispersion were taken from reference. The structures were solved by direct methods (SHELXS).[15] All final refinements were carried out by full-matrix least-squares using anisotropic displacement parameters for all non-hydrogen atoms. Hydrogen atoms were introduced in calculated positions and only one overall isotropic displacement parameter was refined. All crystallographic data and diffraction parameters are listed in Table 1.

The X-ray powder diffraction pattern were recorded at room temperature on a vertical Philips PW1050/25 goniometer mounted in the Bragg–Brentano configuration ($\theta, 2\theta$) using Mn-filtered Fe-K_α radiation.

5. Supplementary material

CCDC-210718 contains the supplementary crystallographic data for this paper. These data can be obtained free of charge at www.ccdc.cam.ac.uk/conts/retrieving.html [or from the Cambridge Crystallographic Data Centre, 12, Union Road, Cambridge CB2 1EZ, UK; Fax: (internat.) +44 1223/336 033; E-mail: deposit@ccdc.cam.ac.uk].

Acknowledgements

The authors thank CNRS, the University Paris-Sud, The Tallinn Technical University and the University Pierre et Marie Curie for financial supports.

References

1. Kajzar, F.; Zyss, J. *MCLC S&T, Sec. B: Nonlinear Opt.* **1995**, *9*, 3–24.

2. Lacroix, P. G.; Clement, R.; Nakatani, K.; Zyss, J.; Ledoux, I. *Science* (*Washington, DC, United States*) **1994**, *263*, 658–660.
3. Coradin, T.; Clément, R.; Lacroix, P. G.; Nakatani, K. *Chem. Mater.* **1996**, *8*, 2153–2158.
4. Bénard, S.; Yu, P.; Audière, J. P.; Rivière, E.; Clément, R.; Guilhem, J.; Tchertanov, L.; Nakatani, K. *J. Am. Chem. Soc.* **2000**, *122*, 9444–9454.
5. Lacroix, P. G. *Chem. Mater.* **2001**, *13*, 3495–3506.
6. Clément, R.; Decurtins, S.; Gruselle, M.; Train, C. *Monatshefte fuer Chem.* **2003**, *134*, 117–135.
7. Gruselle, M.; Thouvenot, R.; Malézieux, B.; Train, C.; Gredin, P.; Demeschik, T. V.; Troitskaya, L. L.; Sokolov, V. I. *Chem. Eur. J.* (in press).
8. Pellaux, R.; Schmalle, H. W.; Huber, R.; Fischer, P.; Hauss, T.; Ouladdiaf, B.; Decurtins, S. *Inorg. Chem.* **1997**, *36*, 2301–2308.
9. Andrés, R.; Gruselle, M.; Malézieux, B.; Verdaguer, M.; Vaissermann, J. *Inorg. Chem.* **1999**, *38*, 4637–4646.
10. Malézieux, B.; Andrés, R.; Brissard, M.; Gruselle, M.; Train, C.; Herson, P.; Troitskaya, L. L.; Sokolov, V. I.; Ovseenko, S. T.; Demeschik, T. V.; Ovanesyan, N. S.; Mamed'yarova, I. A. *J. Organomet. Chem.* **2001**, *637–639*, 182–190.
11. Schlafer, H. L.; Glieman, G. *Basic Principles of Ligand Field Theory*; John Wiley and Sons: New York, 1969.
12. Shriver, D. F.; Atkins, P. W.; Langford, C. H. *Inorganic Chemistry*; Oxford University Press: Oxford, Melbourne, Tokyo, 1990.
13. Bailar, J. C.; Jones, E. M. *Inorg. Synth.* **1939**, *1*, 37–38.
14. Kauffman, G. B.; Takahashi, L. T.; Sugisaka, N. *Inorg. Synth.* **1966**, *8*, 207–210.
15. Sheldrick, G. M. *SHELXL97*; University of Göttingen: Germany, 1997.